A New Schiff Base Epoxy Oligomer Resin: Synthesis, Characterization, and Thermal Decomposition Kinetics

İsmet Kaya,[1] Fatih Doğan,[2] Murat Gül[1]

[1]*Department of Chemistry, Çanakkale Onsekiz Mart University, Çanakkale 17020, Turkey*
[2]*Secondary Science and Mathematics Education, Faculty of Education, Çanakkale Onsekiz Mart University, Çanakkale 17100, Turkey*

Received 23 June 2010; accepted 29 November 2010
DOI 10.1002/app.33843
Published online 11 April 2011 in Wiley Online Library (wileyonlinelibrary.com).

ABSTRACT: Oligo{2,2′-{1,4-phenylenebis[nitrilomethylylidene]}bis(6-methoxyphenol)} (OPNMMP) was synthesized from *o*-vanillin and *p*-phenylene diamine by oxidative polycondensation with NaOCl in an aqueous alkaline. Then, a new Schiff Base epoxy oligomer resin, OPNMMP–epichlorohydrine (EPC), was produced with EPC. The structures of the resulting compounds were confirmed by Fourier transform infrared spectroscopy, ultraviolet–visible spectroscopy, ^{1}H-NMR, and ^{13}C-NMR. Further characterization processes were preformed by thermogravimetry (TG)–differential thermal analysis, gel permeation chromatography, and solubility testing. Also, the kinetics of the thermal decomposition of OPNMMP–EPC were investigated by thermogravimetric analysis. The TG curves showed that the thermal decomposition of OPNMMP–EPC occurred in one stage. The kinetic parameters related to the decomposition kinetics of OPNMMP–EPC were obtained from TG curves with the following methods: Friedman, Flynn–Wall–Ozawa, Kissinger, invariant kinetic parameter, and Coats–Redfern (CR), under an N_2 dynamic atmosphere and different heating rates (5, 10, 15, and 20°C/min). The mechanism function and pre-exponential factor were also determined by a master plots method. The apparent activation energies of the thermal decomposition were calculated from these methods for OPNMMP–EPC. The analysis of the results obtained by the CR and master plots methods showed that the decomposition mechanism of OPNMMP–EPC in N_2 was a deceleration-type mechanism. © 2011 Wiley Periodicals, Inc. J Appl Polym Sci 121: 3211–3222, 2011

Key words: oligomers; synthesis; thermogravimetric analysis (TGA)

INTRODUCTION

Oxidative polycondensation method is simply the reaction of compounds, including active functional groups (e.g., —OH, —NH_2, —CHO, —COOH), in their structure. The oxidative polymerization reaction is usually preformed with different oxidants, such as sodium hypochlorite (NaOCl), H_2O_2, and air in aqueous alkaline or acidic media. The main advantage of this method is the use of easily found, cheap, and simple structured oxidants. Many studies on oxidative polymerization and the reaction mechanisms of polyphenols have been reported.[1–3] Schiff-base-substituted oligomers or polymers, which include azomethine (—CH=N—) and active hydroxyl (—OH) groups, have been used in various fields, including electrochemical cells and materials resistant to high energy, because of their useful properties, including paramagnetism and semiconductivity. They have also been used to prepare compounds with resistance to high temperature, thermostabilizatiors,[4] graphite materials,[5] and antistatic materials.[6] The halogen derivatives of oligophenols are composite materials, such as lead-storing battery cathodes, which are resistant to flame and specific detergents.[7] In addition, Schiff base oligomers or polymers can have antimicrobial properties against some bacteria. All azomethine polymers show a remarkable thermal stability. Nonconjugated polymers are white or cream in color and have thermal stabilities of about 300°C under N_2 and 250°C under an air atmosphere. Aromatic azomethine polymers are yellow, orange, red, brown, or black products, with thermal stabilities up to 500–550°C under N_2 and 430–480°C under an air atmosphere. On the other hand, the kinetics of thermal decomposition are an important tool in predicting the behavior of polymers under varied environmental conditions and are also helpful in determining the strength of various bonds in the polymer backbone chain and, hence, mechanism of the decomposition reaction. Several studies have shown that nonisothermal thermogravimetry (TG) is a powerful tool for characterizing the thermal behavior of polymers.[8,9] Doğan et al.[10] investigated the thermal behavior and kinetic

Correspondence to: F. Doğan (fatihdogan@comu.edu.tr).

parameters, such as the activation energy (E), and decomposition mechanisms of azomethine-based phenol polymer using different methods on the basis of multiple heating rates (βs) under a nitrogen atmosphere by TG/DTG and differential thermal analysis data.[10] The thermal decomposition processes of some phenol polymer–metal complexes were studied by El-Shekeil et al.[11] and Kaya et al.[12] The decomposition mechanism and kinetic parameters of an epoxy with isoconversional and multivariate nonlinear regression methods was also reported by Budrugeac and Segal.[13]

In this study, we investigated the effect of different reaction parameters, such as temperature, time, and initial concentration of NaOCl in an alkaline medium, on the synthesis of oligo{2,2′-{1,4-phenylenebis[nitrilomethylylidene]}bis(6-methoxyphenol)} (OPNMMP). The kinetic parameters, including E, the decomposition or integral function of conversion [$g(\alpha)$], and preexponential factor (A) of thermal decomposition, of OPNMMP–epichlorohydrine (EPC) were also calculated by the Friedman (FR), Flynn–Wall–Ozawa (FWO), Kissinger, Coats–Redfern (CR), and invariant kinetic parameter (IKP) methods from TG curves.

EXPERIMENTAL

Materials

Benzene, *o*-vanillin, *p*-phenylenediamine, methanol, ethanol, toluene, ethyl acetate, CH_2Cl_2, $CHCl_3$, CCl_4, acetone, hexane, tetrahydrofuran (THF), dimethylformamide (DMF), dimethyl sulfoxide (DMSO), H_2SO_4 (98%), KOH, NaOH, EPC, and hydrochloric acid (HCl, 37%) were supplied from Merck Chemical Co. (Darmstatd, Germany), and they were used as received. NaOCl (30% aqueous solution) was supplied from Paksoy Chemical Co. (Adana, Turkey).

Preparation of 2,2-{1,4-phenylenebis[nitrilomethylylidene]}bis(6-methoxyphenol)

PNMMP was prepared with the condensation reaction of *o*-vanillin (10.88 g, 0.08 mol) and *p*-phenylenediamine (4.32 g, 0.04 mol) by boiling under reflux for 3 h in methanol of 75 mL (Scheme 1). The precipitated PNMMP was filtered and recrystallized from methanol and dried in vacuum desiccators.

^{1}H-NMR (DMSO, δ, ppm): 13.21 (s, 1H, —OH), 9.03 (s, 1H, —CH=N—), 7.55 (s, 4H, Ar—Ha), 7.27 (d, 1H, Ar—Hb), 6.93 (m, 1H, Ar—Hc), 7.15 (d, 1H, Ar—Hd), 3.84 (s, 3H, —OCH_3). ^{13}C-NMR (DMSO, δ, ppm): 151.01 (C1-ipso), 148.38 (C2-ipso), 116.10 (C3), 119.14 (C4), 124.37 (C5), 119.74 (C6-ipso), 163.77 (C7), 146.97 (C8-ipso), 123.02 (C9), 56.36 (C10).

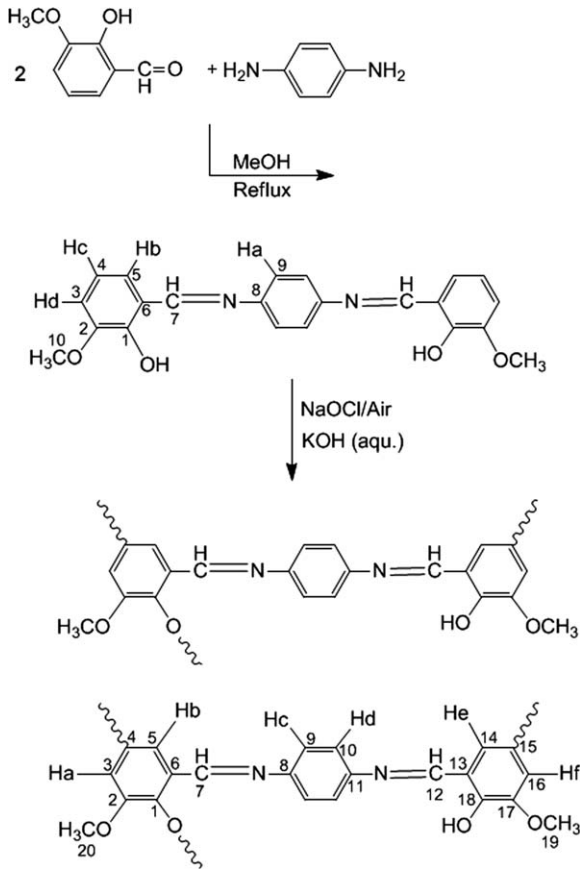

Scheme 1 Synthesis of PNMMP and OPNMMP.

Synthesis of OPNMMP

OPNMMP was synthesized from the oxidative polycondensation reaction of PNMMP in a water solution of NaOCl (30%) (Scheme 1).[12] PNMMP (0.352 g, 0.001 mol) was dissolved in an aqueous solution of KOH (10%, 0.056 g, 0.001 mol) and placed into a 50-mL, three-necked, round-bottom flask. The flask was fitted with a condenser, a thermometer, a stirrer, and an addition to the funnel containing NaOCl. After heating to 30°C, NaOCl was added dropwise to this solution for about 20 min. The reaction mixtures were stirred at various temperatures and times (see Table II, shown later). Then, the mixtures were cooled to room temperature, and 0.001 mol of HCl (37%) was added. Unreacted monomer was separated from the reaction product by washing with $CHCl_3$. The mixture was filtered and washed with hot water (3 × 25 mL) to separate the mineral salts and then dried in the oven at 110°C.

^{1}H-NMR (DMSO, δ, ppm): 13.91 (s, 1H, —OH), 13.20 (s, 1H, —OH), 9.03 (s, 1H, —CH=N—), 8.85 (s, 1H, —CH=N—), 7.04 (d, 1H, Ar—Ha), 7.26 (d, 1H, Ar—Hb), 7.55 (d, 2H, Ar—Hc), 6.63 (d, 2H, Ar—Hd), 7.22 (d, 1H, Ar—He), 6.86 (t, 1H, Ar—Hf), 3.84 (s, 3H, —OCH_3), 3.81 (s, 3H, —OCH_3), 7.14 (t, 1H, terminal proton), 6.93 (t, 1H, terminal proton). ^{13}C-NMR

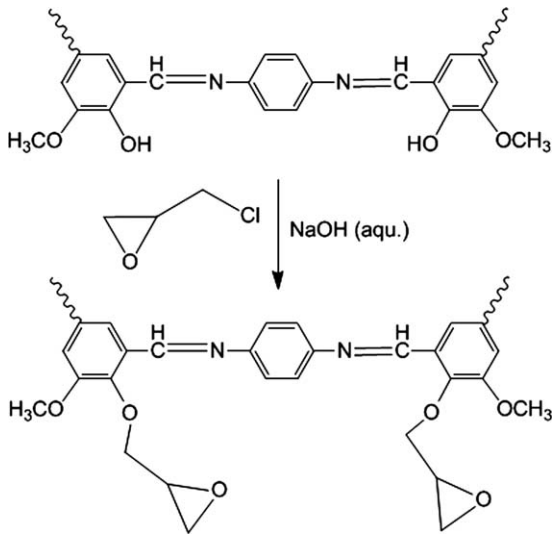

Scheme 2 Synthesis of OPNMMP–EPC.

(DMSO, δ, ppm): 151.02 (C1-ipso), 149.21 (C2-ipso, C17-ipso), 114.60 (C3), 136.03 (C4-ipso), 119.15 (C5), 119.75 (C6-ipso), 163.77 (C7), 148.38 (C8-ipso), 122.88 (C9), 123.03 (C10), 148.26 (C11-ipso), 157.83 (C12), 119.99 (C13-ipso), 124.38 (C14), 123.82 (C15-ipso), 118.72 (C16), 150.75 (C18-ipso), 56.36 (C19), 56.27 (C20), 115.00 and 116.10 (new peaks for the C—C coupling system).

Synthesis of OPNMMP–EPC

A three-necked flask (0.1-L capacity) equipped with a condenser, magnetic stirrer, thermometer, and dropping funnel was charged with Schiff base oligomer (5 g) and EPC (12.5 g, 0.13 mol). The reaction mixture was stirred at temperature 40°C under nitrogen atmosphere for 1 h. Then, the reaction temperature was raised up to reflux at about 90°C. A concentrated solution of 50% sodium hydroxide (1 g or 0.026 mol in 2 mL of water) was transferred to a dropping funnel and added to the reaction flask over 2 h with stirring (Scheme 2). The obtained resins were isolated under pressure with a rotary evaporator and were then dissolved in THF. The solution was filtered to remove the salt. The excess EPC and THF were removed by distillation under reduced pressure.

The epoxy value of resin was determined by an analytical method based on back-titration and was found to be 17%.[14]

Characterization techniques

The infrared spectra were measured on a PerkinElmer Spectrum One Fourier transform infrared (FTIR) system (Canakkale, Turkey) with a universal attenuated total reflection sampling accessory within the wavelengths 4000–550 cm^{-1}. PNMMP, OPNMMP, and OPNMMP–EPC were also characterized by with ^{1}H-NMR and ^{13}C-NMR spectra (Bruker Avance DPX, Ankara, Turkey, 400 and 100.6 MHz, respectively) recorded at 25°C in hexadeuterated DMSO. Tetramethylsilane was used as an internal standard. Thermal data were obtained with a PerkinElmer Diamond thermal analyzer. The TG–differential thermal analysis measurements were made between 15 and 1000°C (under N_2, $\beta = 5$, 10, 15, and 20°C/min). Gel permeation chromatography (GPC) analyses were performed at 30°C with DMF/methanol (4/1 v/v) as an eluent at a flow rate of 0.4 mL/min. A refractive-index detector was used as the detector. The instrument (Shimadzu 10AVp series HPLC–GPC system, Canakkale, Turkey) was calibrated with a mixture of polystyrene standards (Polymer Laboratories; peak molecular weights = 162–189,300) with GPC software for the determination of the number-average molecular weight (M_n), weight-average molecular weight (M_w), and polydispersity index (PDI) of the polymer samples. For GPC investigations, we used a Macherey-Nagel GmbH and Co. (Germany) (100 Å and 7.7-nm diameter loading material) 3.3-mm inside diameter × 300-mm columns.

Kinetic methods

The application of dynamic TG methods holds great promise as a tool for unraveling the mechanisms of the physical and chemical processes that occur during polymer decomposition. In this article, integral isoconversional methods were used to analyze the nonisothermal kinetics of OPNMMP–EPC.

The rate of solid-state nonisothermal decomposition reactions is expressed as follows:

$$\frac{d\alpha}{dT} = \left(\frac{A}{\beta}\right) \exp\left(\frac{-E}{RT}\right) f(\alpha) \tag{1}$$

Rearranging eq. (1) and integrating both sides of the equation leads to the following expression:

$$g(\alpha) = \left(\frac{A}{\beta}\right) \int_{T_0}^{T} \exp\left(\frac{-E}{RT}\right) dT = \left(\frac{AE}{\beta R}\right) p(u) \tag{2}$$

where $p(u) = \int_{\infty}^{u} -\left(\frac{e^{-u}}{u^2}\right) du$ and $u = E/RT$.

In the previous equations, α is the conversion at time t, A is the pre-exponential factor (min^{-1}), and $f(\alpha)$ is the differential conversion function.

FWO method[15,16]

This method is derived from the integral method. The technique assumes that A, $f(\alpha)$, and E are

TABLE I
Algebraic Expression for the Most Frequently Used Mechanisms of Solid-State Processes

Number	Mechanisms	Symbol	$f(\alpha)$	$g(\alpha)$
Sigmoidal curves				
1	N and G ($n = 1$)	A_1	$(1-\alpha)$	$[-\ln(1-\alpha)]$
2	N and G ($n = 1.5$)	$A_{1.5}$	$(3/2)(1-\alpha)[-\ln(1-\alpha)]^{1/3}$	$[-\ln(1-\alpha)]^{2/3}$
3	N and G ($n = 2$)	A_2	$2(1-\alpha)[-\ln(1-\alpha)]^{1/2}$	$[-\ln(1-\alpha)]^{1/2}$
4	N and G ($n = 3$)	A_3	$3(1-\alpha)[-\ln(1-\alpha)]^{2/3}$	$[-\ln(1-\alpha)]^{1/3}$
5	N and G ($n = 4$)	A_4	$4(1-\alpha)[-\ln(1-\alpha)]^{3/4}$	$[-\ln(1-\alpha)]^{1/4}$
Deceleration curves				
6	Diffusion, 1D	D_1	$1/(2\,\alpha)$	α^2
7	Diffusion, 2D	D_2	$1/(\ln(1-\alpha))$	$(1-\alpha)\ln(1-\alpha)+\alpha$
8	Diffusion, 3D	D_3	$1.5/[(1-\alpha)^{-1/3}-1]$	$(1-2\alpha/3)-(1-\alpha)^{2/3}$
9	Diffusion, 3D	D_4	$[1.5(1-\alpha)^{2/3}][1-(1-\alpha)^{1/3}]^{-1}$	$[1-(1-\alpha)^{1/3}]^2$
10	Diffusion, 3D	D_5	$(3/2)(1+\alpha)^{2/3}[(1+\alpha)^{1/3}-1]^{-1}$	$[(1+\alpha)^{1/3}-1]^2$
11	Diffusion, 3D	D_6	$(3/2)(1-\alpha)^{4/3}[[1/(1-\alpha)^{1/3}]-1]^{-1}$	$[[1/(1-\alpha)]^{1/3}-1]^2$
12	Contracted geometry shape (cylindrical symmetry)	R_2	$2(1-\alpha)^{1/2}$	$2[1-(1-\alpha)^{1/2}]$
13	Contracted geometry shape (sphere symmetry)	R_3	$3(1-\alpha)^{2/3}$	$3[1-(1-\alpha)^{1/3}]$
Acceleration curves				
14	Mample power law	P_1	1	α
15	Mample power law ($n = 2$)	P_2	$2\alpha^{1/2}$	$\alpha^{1/2}$
16	Mample power law ($n = 3$)	P_3	$(1.5)\alpha^{2/3}$	$\alpha^{1/3}$
17	Mample power law ($n = 4$)	P_4	$4\alpha^{3/4}$	$\alpha^{1/4}$
18	Mample power law ($n = 2/3$)	$P_{3/2}$	$2/3(\alpha)^{-1/2}$	$\alpha^{3/2}$
19	Mample power law ($n = 3/2$)	$P_{2/3}$	$3/2(\alpha)^{1/3}$	$\alpha^{2/3}$
20	Mample power law ($n = 3/4$)	$P_{3/4}$	$4/3(\alpha)^{-1/3}$	$\alpha^{3/4}$

N = nucleation; G = growth; 1D = one-dimensional diffusion; 2D = two-dimensional diffusion; 3D = three-dimensional diffusion.

independent of the absolute temperature (T); when A and E are independent of α, eq. (2) may be integrated to give the following equation in logarithmic form:

$$\log g(\alpha) = \log(AE/R) - \log\beta + \log p(E/RT) \quad (3)$$

where R is the gas constant (8.314 J mol^{-1} K^{-1}). With Doyle's approximation[17] for the integral, which allows for $E/RT > 20$, eq. (3) can be simplified as follows:

$$\log\beta = \log(AE/R) - \log[g(\alpha)] - 2.315 - 0.4567E/RT \quad (4)$$

CR method[18]

The CR method is also an integral method, and it involves the thermal decomposition mechanism. With an asymptotic approximation for the solution of eq. (2), the following equation can be obtained:

$$\ln\left(\frac{g(\alpha)}{T^2}\right) = \ln\left(\frac{AR}{E\beta}\right) - \frac{E}{RT} \quad (5)$$

The expressions of $g(\alpha)$[19] for different mechanism are listed Table I, and E for the decomposition mechanism can be obtained from the slope of a plot of $\ln[g(\alpha)/T^2]$ versus $1000/T$.

FR method[20]

The FR method provides the following expression for thermal decomposition kinetic studies based on a basic Arrhenius equation:

$$\ln\left(\frac{d\alpha}{dt}\right) = \ln(A) + n\ln(1-n) - \frac{E}{RT} \quad (6)$$

where T is the absolute temperature (K). The plot of $\ln(d\alpha/dt)$ versus $1/T$ should be linear with the slope E/R, from which E can be obtained.

Kissinger method[21]

The Kissinger method for calculating E uses the maximum decomposition temperature (T_{max}) at which the rate of mass loss is the highest. Because the highest rate happens when $d(d\alpha/dt)/dt = 0$, the differentiation of the equation $f(\alpha) = (1-\alpha)^n$ (where n = reaction order) gives

$$\frac{E\beta}{RT_{max}^2} = An(1-\alpha_{max})^{1-n}\exp(-E/RT_{max}) \quad (7)$$

The Kissinger method assumes that the decomposition product $n(1-\alpha_{max})^{n-1}$ is independent of β. So, the following equation can be deduced:

$$\ln\frac{\beta}{T_{max}^2} = \left\{\ln\frac{AE}{R} + \ln[n(1-\alpha_{max})^{n-1}]\right\} - \frac{E}{RT_{max}} \quad (8)$$

The E value can be calculated from the slope of a plot of $\ln(\beta/T_{max}^2)$ versus $1000/T_{max}$.

IKP method[22]

The thermal decomposition of a solid in an heterogeneous process is accompanied by the release of gaseous products and can usually be characterized by several forms of the function $f(\alpha)$, given in Table I. The IKP method is based on the relation of the compensation effect, which is described by the E values, and A, obtained from various conversion functions with one of the different methods (differential or integral methods, etc.) for TG curves. To apply this method, $\alpha = \alpha(T)$ curves for several heating rates (β_v's; $v = 1, 2, 3\ldots$) are recorded, and the activation parameters E and A for a set of conversion functions [$f_j(\alpha)$, $j = 1,2,3\ldots$], at each β are calculated with an integral method, a differential method, and another method. In this study, the CR method was used to integrate eq. (1). It led to the following relations:

$$\ln\frac{g_j(\alpha_{iv})}{T_{iv}^2} \cong \ln\frac{A_{jv}R}{\beta_v E_{jv}} - \frac{E_{jv}}{RT_{iv}} \quad (9)$$

with $g_j(\alpha) = \int_0^\alpha \frac{d\alpha}{f_j(\alpha)}$.

where i is data point; β and v are the heating rate and its number, respectively; and j is the number of the conversion function and is between 1 and 20. A plot of $\ln[\frac{g_j(\alpha_{iv})}{T_{iv}^2}]$ versus $\frac{1}{T_{iv}}$ for a given analytical form of $g(\alpha)$ should be a straight line. We used the 20 different conversion functions given in Table I for $f(\alpha)$ and $g(\alpha)$ in eq. (9). Twenty couples (E_{jv}, A_{jv}) of OPNMMP–EPC per β are obtained with the CR method. The application of the IKP method is based on the study of the compensation effect. If a compensation effect is observed, a linear relation defined by eq. (10) for each β is obtained. One shows by plotting ln A versus E that a compensation effect is observed for each β. Thus, with the relation of the compensation effect, for each β, the compensation parameters (α^*, β^*) are determined:

$$\ln A = \alpha^* + \beta^* E \quad (10)$$

which leads to the supercorrelation relation:

$$\alpha^* = \ln A_{int} - \beta^* E_{int} \quad (11)$$

where α^* and β^* are constants (the compensation effect parameters), A_{int} and E_{int} are invariant activation energy and invariant pre-exponential factor, respectively. A plot α^* versus β^* is actually a straight line whose parameters allow for the evaluation of the invariant activation parameters. Thus, the values of invariant E and invariant A can be calculated from the slopes and intercepts of the curves.

Determination of the kinetic model by the master plots method

Using a reference at point $\alpha = 0.5$ and according to eq. (2), one gets

$$g(\alpha) = \left(\frac{AE}{\beta R}\right)p(u_{0.5}) \quad (12)$$

where $u_{0.5} = E/RT$. When eq. (2) is divided by eq. (12), the following equation is obtained:

$$\frac{g(\alpha)}{g(0.5)} = \frac{p(u)}{p(u_{0.5})} \quad (13)$$

Plots of $g(\alpha)/g(0.5)$ against α correspond to the theoretical master plots of various $g(\alpha)$ functions.[23,24] To draw the experimental master plots of $P(u)/P(u_{0.5})$ ($P(u)$ is labeled as temperature integral, also $P(u_{0.5})$ is temperature integral at point $\alpha = 0.5$.) against α from experimental data obtained under different βs, an approximate formula[25] of $P(u)$ with high accuracy is used: $P(u) = \exp(-u)/[u(1.00198882u + 1.87391198)]$. Equation (13) indicates that for a given α, the experimental values of $g(\alpha)/g(\alpha_{0.5})$ are equivalent when an appropriate kinetic model is used. Comparing the experimental master plots with the theoretical ones concludes the kinetic model.

RESULTS AND DISCUSSION

Optimum reaction conditions of OPNMMP

The oxidative polycondensation reaction conditions of the synthesis of PNMMP with a 30% NaOCl solution in an aqueous alkaline medium are given in Table II. The yield of OPNMMP was found to be 83% for the NaOCl oxidant for 1 h at 60°C. It is shown clearly in Table II that the amount of products decreased with increasing temperature. Under the same conditions, when a molar amount of NaOCl

TABLE II
Parameter Related to the Oxidative Polycondensation Reaction of PNMMP[a]

Run	$[KOH]_0$ (mol/L)	$[NaOCl]_0$ (mol/L)	Temperature (°C)	Time (h)	Yield of OPNMMP (%)
1	0.027	0.027	50	1	76
2	0.027	0.027	60	1	83
3	0.027	0.027	70	1	80
4	0.027	0.027	80	1	73
5	0.027	0.027	90	1	62
6	0.081	0.027	60	1	96
7	0.054	0.054	60	1	83
8	0.027	0.054	60	1	95
9	0.027	0.081	60	1	98
10	0.054	0.054	60	3	79
11	0.054	0.054	60	5	70

[a] The initial concentration of PNMMP was used as 0.027 mol/L.

TABLE III
M_n, M_w, and PDI Values and Percentages of Oxidative Polycondensation Products of OPNMMP

	Molecular weight distribution parameters														
	Total			Fraction I				Fraction II				Fraction III			
Compound	M_n	M_w	PDI	M_n	M_w	PDI	%	M_n	M_w	PDI	%	M_n	M_w	PDI	%
OPNMMP[a]	1300	1500	1.154	900	1050	1.167	90	1,900	2,100	1.105	5	60,000	66,500	1.108	5
OPNMMP[b]	1500	1900	1.267	1100	1600	1.455	95	38,600	45,400	1.176	5	—	—	—	—

[a] NaOCl oxidant.
[b] Air oxidant.

increased in a two-coating dependence on PNMMP, the total yield changed from 83 to 95%. The yield of OPNMMP was 98% under optimum conditions ($[PNMMP]_0 = [KOH]_0 = 0.027$ mol/L, and $[NaOCl]_0 = 0.081$ mol/L at 60°C and 1 h).

Solubility

The experiments for the optimum polymerization conditions of the synthesis of PNMMP were performed at various temperatures and times with NaOCl as an oxidant. As a result of these experiments, oligoazomethine, which changed colored from light brown to black, was obtained. OPNMMP was dark brown in powdered form, and it was completely soluble in organic solvents, such as DMF, THF, and DMSO. However, it was insoluble in hexane, benzene, toluene, ethyl acetate, CH_2Cl_2, $CHCl_3$, CCl_4, and acetone.

Structure of OPNMMP

GPC analyses of OPNMMP were performed at 30°C with DMF/methanol (v/v, 4/1) as an eluent at a flow rate of 0.4 mL/min. The M_n, M_w, and PDI values of OPNMMP were found to be 1300 g/mol, 1500 g/mol, and 1.154 and 1500 g/mol, 1900 g/mol, and 1.267, for the NaOCl and air oxidants, respectively (Table III). Three peaks were observed in the chromatogram of OPNMMP. For the NaOCl oxidant, 95 mass % of OPNMMP was low molecular weight [fraction I (90): M_n = 900 g/mol, M_w = 1050 g/mol, and PDI = 1.167; fraction II (5): M_n = 1900 g/mol, M_w = 2100 g/mol, and PDI = 1.105), but 5 wt % was high molecular weight (fraction III: M_n = 60,000 g/mol, M_w = 66,500 g/mol, and PDI = 1.108). For the air oxidant, 95 mass % of OPNMMP was low molecular weight (fraction I: M_n = 1100 g/mol, M_w = 1600 g/mol, and PDI = 1.455) but 5 wt % was high molecular weight (fraction II: M_n = 38,600 g/mol, M_w = 45,400 g/mol, PDI = 1.176). Because of the increasing the molecular weight, together with the broadening of PDI, NMR analyses failed to give valuable information for the characterization of these compounds. However, GPC analysis showed that new oligomer was formed, and the traces shifted to higher molecular weights. However, the molecular weights measured by GPC on the basis of PS standards should be taken as the minimum estimation because of the highly branched or comblike structure of the obtained oligoazomethine.

Ultraviolet–visible (UV–vis) spectroscopic studies were carried out with DMSO solutions of the PNMMP and OPNMMP. In the spectrum of PNMMP, K bands of phenol and C_6H_5—N= were observed at 237 and 284 nm, respectively. The R band and —CH=N— group of PNMMP were observed at 353 and 386 nm, respectively. Maximum wavelengths (λ_{max}) values of OPNMMP were observed at 253, 379, and 385 nm. In the UV–vis spectrum of OPNMMP, K and R bands were observed at 253 and 379 nm, respectively. The band of the —CH=N— group was observed at 385 nm. The FTIR spectral data of PNMMP, OPNMMP, and OPNMMP–EPC are given in Table IV. In the FTIR spectra of PNMMP, OPNMMP, and OPNMMP–EPC, bands of the —OH and —CH=N groups were observed at 3342 and 1604, 3352 and 1606, and 3348 and 1604 cm^{-1}, respectively. Also, the band of epoxy rings was observed at 1051 cm^{-1}.

To identify the structures of the monomer, oligomer, and epoxy resin, the ^{1}H-NMR and ^{13}C-

TABLE IV
FTIR Spectral Data of the PNMMP, OPNMMP, and OPNMMP–EPC Compounds

	Wave number (cm^{-1})				
Compound	—OH	—CH=N	—C=C	—C—O	EPC ring
PNMMP	3342	1604	1578, 1508, 1460	1249	—
OPNMMP	3452	1606	1576, 1508, 1464	1252	—
OPNMMP–EPC	3348	1604	1586, 1515, 1482	1264	1051

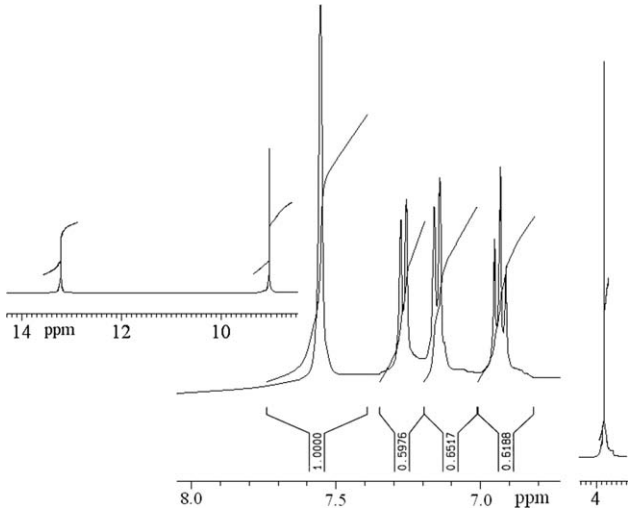

Figure 1 ^{1}H-NMR spectrum of PNMMP.

NMR spectra of all compounds were recorded in hexadeuterated DMSO and are given in Figures 1–4. In the ^{1}H-NMR spectra of PNMMP and OPNMMP, the signals of phenyl —OH and —CH=N groups are shown at 13.21 and 9.03 and 13.91 and 8.85 ppm, respectively. The FTIR spectral data and the results of the ^{1}H-NMR and ^{13}C-NMR spectra of the OPNMMP confirmed each other. Crosslinking in the polymer structure is expected in those cases where the ortho and para positions in the corresponding monomer structure are unsubstituted. ^{13}C-NMR studies of OPBNMMP indicated that the linkage between phenyl rings were para positions because its ortho positions were substituted with methoxy groups (Fig. 3). As shown in the ^{13}C-NMR spectra of the oligomer, the peak at 136 ppm, assigned to C—C

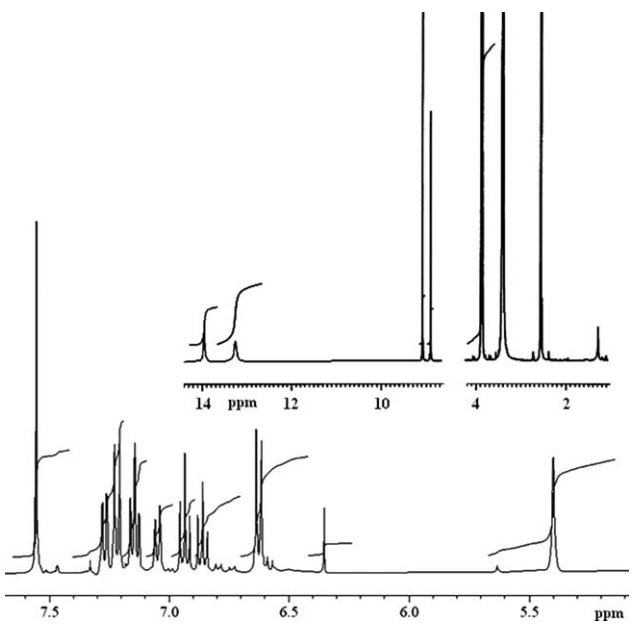

Figure 2 ^{1}H-NMR spectrum of OPNMMP.

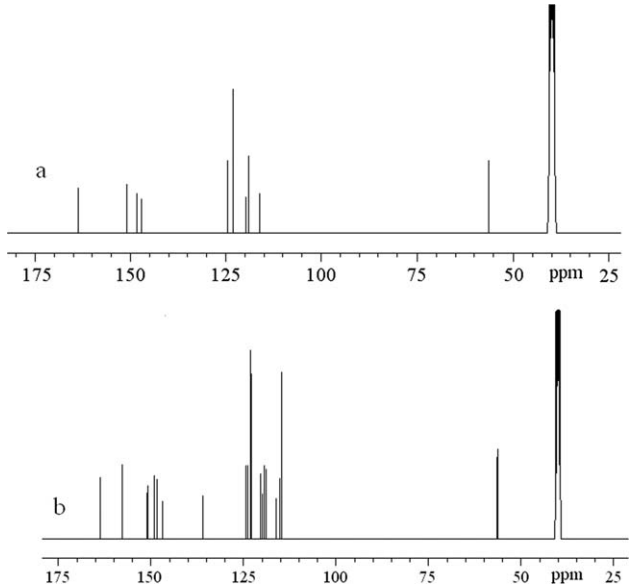

Figure 3 ^{13}C-NMR spectra of PNMMP and OPNMMP.

coupling, was not present in the case of the monomer. Proton signals of the epoxy groups of resin (—OCH_2, —CH—, and —CH_2—) were observed at 2.63, 4, and 2.98 ppm, respectively. Moreover, ^{1}H-NMR spectra could be used to determine the epoxy functionality of the epoxy resin through the integration of the characteristic signals. This procedure was applied to determine the chemical compositions for the graft and block copolymers.[26] Accordingly, the same procedure was applied hereafter to determine the epoxy functionality of glycidyl ethers. In this respect, the analysis was based on the integration of two signals, namely, those at 4 ppm (assigned to the CH proton of the oxirane ring) and at 13.91 ppm (assigned to unreacted OH protons). The ratio of

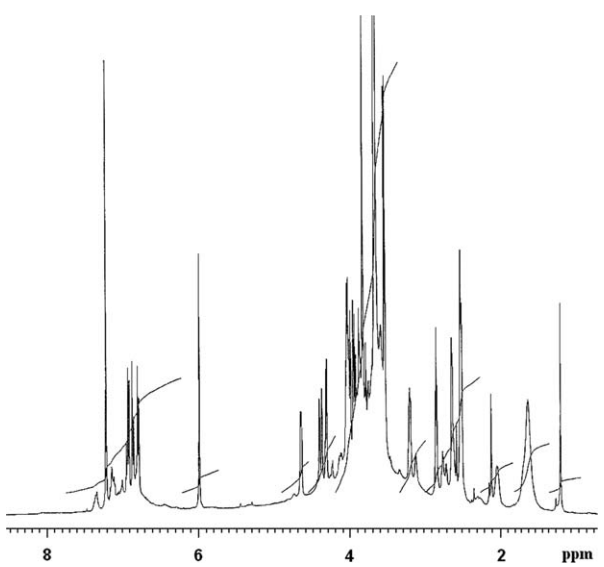

Figure 4 ^{1}H-NMR spectrum of OPNMMP–EPC.

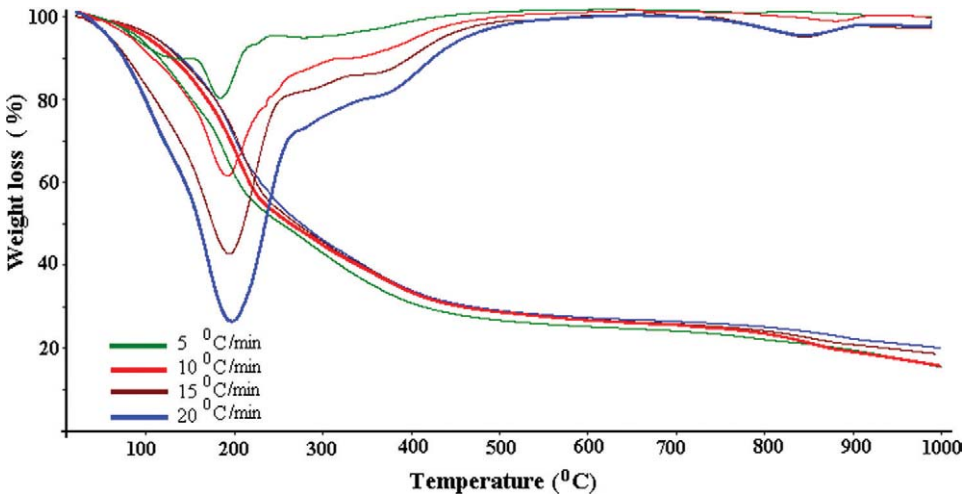

Figure 5 TG–DTG curves of OPNMMP–EPC. [Color figure can be viewed in the online issue, which is available at wileyonlinelibrary.com.]

integration of these protons signals showed that each two hydroxyl groups of the resins reacted with EPC. Also, the signals of the hydroxyl groups disappeared from the spectrum. These cases were ascribed to reactions ending with EPC.

Thermal decomposition process

Kinetic parameters related to the solid-state decomposition process can be calculated by isothermal or nonisothermal methods. A kinetic calculation performed by isothermal methods results in a small amount of data from TG curves, and it is often quite difficult to interpret from these curves. On the other hand, several data, such as all stages of the solid-state decomposition process, related temperatures, and percentage conversion degree, can be clearly observed from a single nonisothermal TG curve. Nonisothermal TG is, therefore, often preferred over isothermal TG in calculations of the kinetic parameters of the solid-state decomposition process. Nonisothermal TG can be classified two groups. First, there are methods that are applied to several βs, such as the Freidman, Ozawa, and Kissinger methods. Second, there are methods that are applied to a single β, such as the CR and MacCallum Taner methods. These methods are highly dependent on the reaction order and conversion degree that takes part in $g(\alpha)$. E values are calculated either with special values in the reaction order or with some assumptions made. A special software program can handle this obstacle. On the other hand, E changes to some extent with β. In fact, the grounds of this are still discussed. To put it briefly, it is appropriate to evaluate each method according to its own pros and cons. However, recent authors have often discussed integral methods dependent on a single β at a wide range of temperatures or the isothermal model dependency of these methods. Because of the abovementioned factors, both groups of methods have peculiar constraints with regard to mathematics or feasibility. However, the kinetic parameter of a solid-state decomposition process can be calculated from the methods of both groups. The studies reported in recent years have used all of the methods. Therefore, these methods can be considered complementary to each other as well. The outcomes of different methods can be compared; as a result, more accurate kinetic parameters can be obtained. The thermal decomposition of OPNMMP–EPC was selected for the kinetic study. E of the decomposition process was determined by multiple β kinetics. The typical dynamic TG/DTG thermograms of OPNMMP–EPC under a dynamic nitrogen atmosphere are shown in Figure 5, where the TG curves for the decomposition of an 8–10 mg OPNMMP–EPC sample are shown with 5, 10, 15, and 20°C/min under 60 mL/min nitrogen gas. All of the TG curves of OPNMMP–EPC showed that the thermal decomposition took place mainly in one stage, and the curves shifted to the right-hand side with temperature.

Determination of E, kinetic model [$g(\alpha)$], and A

Several techniques with different approaches have been developed for solving the integral of eq. (2). The four methods carried out in this study were those of FWO, Kissinger, IKP, and CR. The CR method was based on a single β, whereas the other methods were based on multiple βs. First, the isoconversional methods were used to analyze the TG data of OPNMMP–EPC because they were independent of any thermal decomposition mechanisms.

TABLE V
***E* and Correlation Coefficient Values Obtained by Different Methods**

	FWO method		FR method	
Conversion	*E*	*r*	*E*	*r*
0.05	101.5	0.98531	104.9	0.98411
0.1	92.29	0.98942	84.96	0.98631
0.2	84.28	0.98821	85.80	0.98741
0.3	84.10	0.99541	89.29	0.99781
0.4	85.01	0.99561	80.39	0.99231
0.5	84.10	0.99112	84.63	0.99781
0.6	80.82	0.99432	80.81	0.99134
0.7	83.92	0.99213	79.98	0.99411
0.8	81.01	0.99511	80.56	0.99561
0.9	82.10	0.99345	73.66	0.99234
0.95	67.53	0.98113	57.28	0.98451
Mean	84.2		82.02	

E, activation energy (kJ/mol); *r*, correlation coefficient.

The FWO method is an integral method and is independent of the decomposition mechanism. Equation (4) was used, and *E* of OPNMMP–EPC could, therefore, be obtained from a plot of log β against $1000/T$ for a constant degree of conversion because the slope of such a line was given by $-0.456E/RT$. The determined *E* values are listed in Table V, and the average value was 84.2 kJ/mol over the range of α given. On the other hand, the FR method allowed *E* to be determined by the plotting of $\ln[\beta d\alpha/dT]$ against $1000/T$ over a wide range of conversions (Fig. 6). In this study, α values of 0.05–0.95 were chosen to determine the *E* values of OPNMMP–EPC. The results are displayed in Table V. The mean value of *E* of OPNMMP–EPC in N_2 was determined to be 82.02 kJ/mol. This result agreed better with the mean value of *E* obtained by the FWO method.

Like the other methods previously discussed, the Kissinger method was also chosen to study the decomposition kinetics of OPNMMP–EPC because no thermal decomposition mechanism is associated with this method. Equation (8) was used to obtain *E* of OPNMMP–EPC, which we could calculate from the plot of $\ln(\beta/T_{max}^2)$ versus $1000/T_{max}$ and fitting the data to a straight line. The plot of the thermal decomposition stage under N_2 is shown in Figure 7. The *E* value of the thermal decomposition of OPNMMP–EPC were found to be 88.47 kJ/mol; this value was much greater than the related values of OPNMMP–EPC obtained by the other two methods under an N_2 atmosphere.

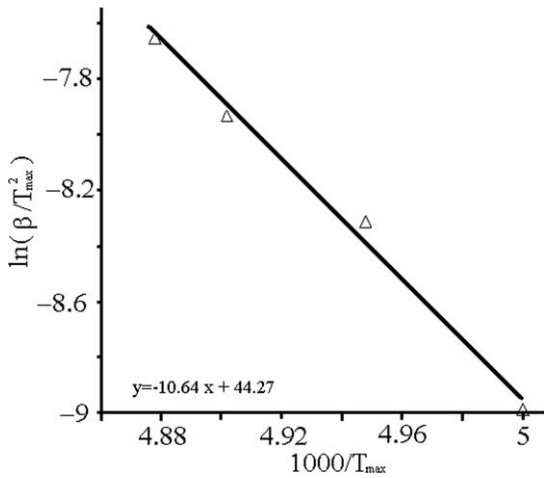

Figure 7 Kissinger plot obtained for OPNMMP–EPC in N_2.

Constant mass loss lines were determined by the measurement of the temperature at a given mass percentage for each rate. In Figure 8, Arrhenius-type plots of the dynamic TG runs are shown for masses ranging from $\alpha = 0.09$ to 0.95 under N_2. Table V summarizes the *E* and correlation coefficient values for the overall mass loss from 5 to 95 mass % under N_2. The results indicate that an acceptable correlation coefficient was always superior to 0.98113.

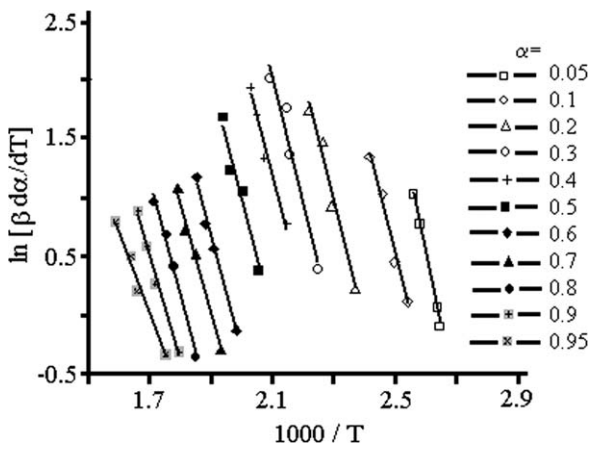

Figure 6 Plot of $\ln[\beta\, d\alpha/dT]$ against $1000/T$ according to Freidman's equation of OPNMMP–EPC.

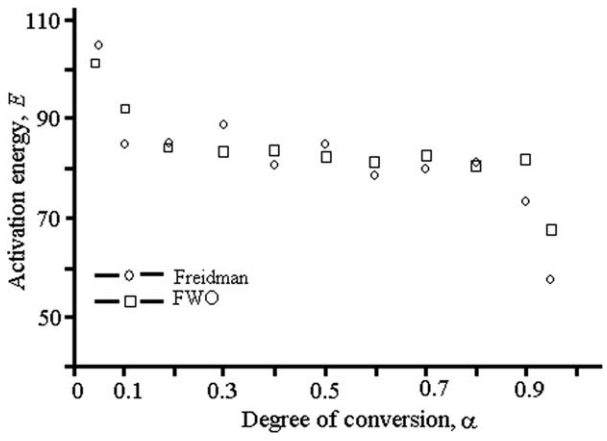

Figure 8 *E* as a function of the degree of conversion for the decomposition process of OPNMMP–EPC as calculated by the FWO and FR methods.

TABLE VI
***E*, *A*, and Correlation Coefficient Values of OPNMMP–EPC Obtained by the CR Method Under an N_2 Atmosphere**

	5°C/min			10°C/min			15°C/min			20°C/min		
	E (kJ/mol)	ln *A*	*r*	*E* (kJ/mol)	ln *A*	*r*	*E* (kJ/mol)	ln *A*	*r*	*E* (kJ/mol)	ln *A*	*r*
A_1	27.61	3.857	0.98321	25.81	2.872	0.98671	25.98	4.071	0.98122	25.56	3.212	0.98211
$A_{1.5}$	15.84	0.488	0.98213	14.57	0.582	0.98891	14.65	0.933	0.99211	14.31	1.036	0.98164
A_2	9.961	−1.371	0.99213	8.958	—1.192	0.99345	8.982	—0.839	0.99421	8.691	–0.713	0.99467
A_3	4.081	−3.671	0.98542	3.341	−3.461	0.98543	3.314	−3.119	0.98511	3.074	−4.471	0.98411
A_4	1.141	−5.652	0.99420	0.533	−5.944	0.99112	0.481	−5.692	0.99648	0.262	−6.092	0.99821
D_1	44.35	7.183	0.99145	41.99	6.795	0.99122	42.28	7.098	0.99131	41.54	7.0123	0.99331
D_2	49.26	8.087	0.99187	46.62	7.591	0.99220	46.97	7.891	0.99054	46.23	7.7910	0.99141
D_3	51.38	7.262	0.99234	48.63	6.723	0.99224	49.00	7.018	0.99286	48.26	6.9129	0.99268
D_4	55.74	8.655	0.99261	52.72	8.018	0.99314	53.17	8.311	0.99343	52.44	8.1964	0.99421
D_5	40.06	3.518	0.99312	37.92	3.221	0.99321	38.16	3.526	0.99432	37.45	3.8811	0.99521
D_6	71.06	13.46	0.99721	67.24	12.51	0.99656	67.80	12.77	0.99521	67.15	11.292	0.99834
R_2	22.43	1.408	0.98612	20.92	1.401	0.98332	21.04	1.736	0.98133	20.60	1.7942	0.98123
R_3	24.03	1.551	0.98874	22.43	1.508	0.98221	22.57	−3.731	0.98641	22.13	1.8991	0.98412
P_1	18.34	0.657	0.99221	17.05	0.738	0.99112	17.13	1.075	0.99611	16.68	1.1413	0.98811
P_2	5.331	−3.391	0.99365	4.579	−3.152	0.99332	4.555	−2.806	0.99850	4.253	−2.718	0.97631
P_3	0.993	−6.019	0.99471	0.442	−6.405	0.99112	0.363	−6.189	0.99124	0.114	−7.156	0.97121
P_4	1.174	−6.319	0.98211	1.656	−5.461	0.98311	1.792	−5.053	0.98121	1.957	−4.721	0.98606
$P_{3/2}$	31.34	4.016	0.97411	29.52	3.867	0.97151	29.71	4.186	0.97641	29.11	4.177	0.97608
$P_{2/3}$	9.611	−1.864	0.98421	8.736	−1.641	0.98657	8.748	−1.301	0.98411	8.401	−1.200	0.98812
$P_{3/4}$	11.83	−1.190	0.98863	10.81	−1.006	0.98321	10.84	−0.659	0.98542	10.47	−0.565	0.98778

r, regression coefficient.

The thermal decomposition of OPNMMP–EPC under N_2 presented the same behavior for the FWO and FR methods. The initial *E* required for initial decomposition was about 101.5 kJ/mol. When 95 mass % of OPNMMP–EPC was lost, *E* decreased to a value of about 57.28 kJ/mol. *E* depended on the conversion degree and usually tended to decrease a small amount according to the increasing decomposition ratio. Then, we assumed that the decomposition stage of OPNMMP–EPC took place only over one mechanism. To determine the decomposition mechanism of OPNMMP–EPC, the CR method was chosen because it involved the mechanisms of the solid-state process. According to eq. (5), *E* for every $g(\alpha)$ function listed in Table I could be calculated at a constant β from the fitting of the $\ln[g(\alpha)/T^2]$ versus $1000/T$ plots. The *E* values and the correlations at constant βs, such as 5, 10, 15, and 20°C/min, are tabulated in Table VI for the thermal decomposition of OPNMMP–EPC.

The latest method using the calculation of kinetic parameters is the IKP method. The application of the IKP method is based on the study of the compensation effect. If a compensation effect is observed, a linear relation defined by eq. (10) for each β, and β is obtained. One shows by plotting ln *A* versus E that a compensation effect is observed for each β. Thus, with the relation of the compensation effect, for each β, the compensation parameters (α^*, β^*) are determined.

$$\ln A = \alpha^* + \beta^* E$$

This leads to a supercorrelation relation.

$$\alpha^* = \ln A_{\text{int}} - \beta^* E_{\text{int}}.$$

The values of α^* and β^* obtained for OPNMMP–EPC are presented in Table VII. Thus, the values of invariant *E* and invariant *A* could be calculated from the slopes and intercepts of the curves.

TABLE VII
Values of α^* and β^* for OPNMMP–EPC Versus β

β (°C/min)	α^*	β^*	*r*
5	0.2568	−4.829	0.99912
10	0.2529	−4.495	0.99843
15	0.2509	−4.404	0.99841
20	0.2488	−4.168	0.99813

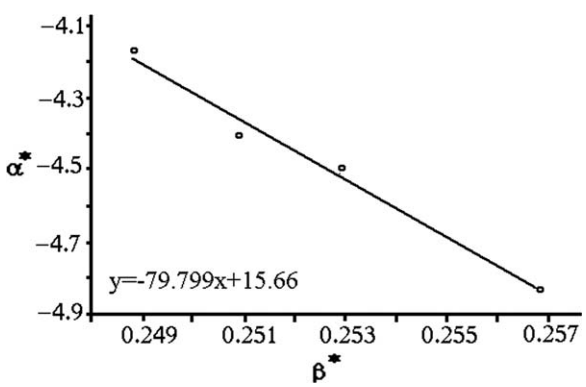

Figure 9 Verifying supercorrelation relation.

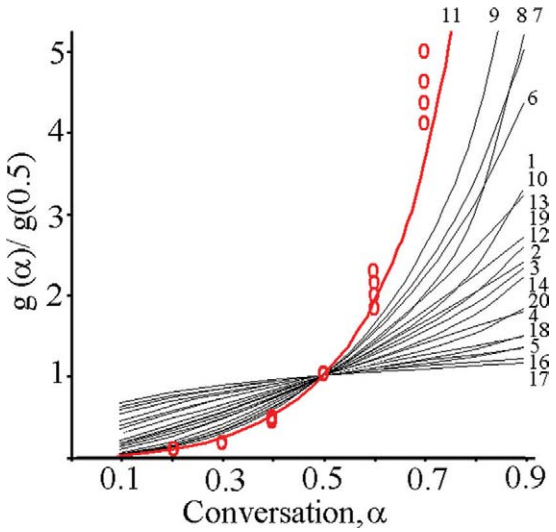

Figure 10 Theoretical and experimental master plots of various kinetic functions. [Color figure can be viewed in the online issue, which is available at wileyonlinelibrary.com.]

A plot of α* versus β* was actually a straight line whose parameters allowed us to evaluate the invariant activation parameters (Fig. 9).

The significance of α* and β* being characteristics of the experimental conditions was demonstrated by Lesnikovich and Levchik.[27] Consequently, the values of invariant E and invariant A calculated from the slope and intercept of the straight line obtained with eq. (11) were found to be 79.799 kJ/mol and 15.66. The regression coefficient of this curve was 0.99830. To determine the mechanism of the decomposition of OPNMMP–EPC, we compared the E values obtained by the methods mentioned previously. According to Table VI, the E values of OPNMMP–EPC in N_2 corresponding to mechanism D_6 were in best agreement with the values obtained by the FR and FWO methods. Notably, at a β of 5°C/min, E corresponding to mechanism D_6 was 71.06 kJ/mol; this was very close to the value of 82.02 kJ/mol obtained by the FR method. The correlation coefficient was also much higher than those of other values. To confirm the conclusions, experimental master plots of $P(u)/P(u_{0.5})$ against α were constructed from the experimental data of the thermal decomposition of OPNMMP–EPC under different βs, and the theoretical master plots of various kinetic functions are all shown in Figure 10.

TABLE VIII
***A* and Correlation Coefficient Values Obtained by the Plotting of ln[β*R*/*E*] Versus ln[*P*(*u*)] Against the Kinetic Functions**

β (K/mol)	ln A (s^{-1})	r
5	14.97	0.9923
10	13.23	0.9898
15	16.83	0.9895
20	15.05	0.9940
Mean	15.02	

r, correlation coefficient.

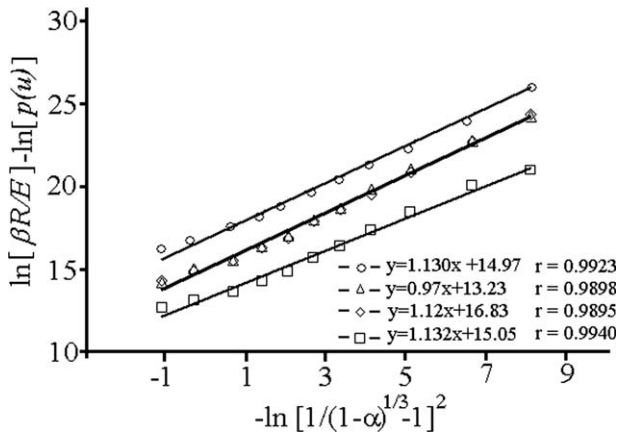

Figure 11 Plot of $\ln[\beta R/E] - \ln[P(u)]$ against $-\ln[1/(1-\alpha)^{1/3} - 1]^2$ for the decomposition stage of OPNMMP–EPC at βs of (○) 5, (▲) 10, (◇) 15, and (□) 20°C/min and their linear-fit drawing (solid lines), respectively.

The comparison of the experimental master plots with theoretical ones indicated that the kinetic process of the thermal decomposition of OPNMMP–EPC agreed well with the D_6 master curve. With the assumption of a D_n law, the experimental data, the expression of the D_n model, and the average reaction energy predetermined were introduced into eq. (2), and the following expression was obtained:

$$\ln[\beta R/E] - \ln[P(u)] = \ln A - \ln[1/(1-\alpha)^{1/3} - 1]^2 \quad (10)$$

We obtained a group of lines by plotting $\ln[\beta R/E] - \ln[P(u)]$ against $-\ln[1/(1-\alpha)^{1/3} - 1]^2$. As shown in Figure 11 and listed in Table VIII, A was calculated from the intercepts of the lines corresponding to various βs.

CONCLUSIONS

A new oligophenol, OPNMMP, and an oligophenol–epoxy derivative, OPNMMP–EPC, were synthesized and characterized by spectroscopic (UV–vis, FTIR, ^{1}H-NMR, and ^{13}C-NMR), analytical and thermogravimetric analyses and thermal studies. Under the optimum reaction conditions, the yield of OPNMMP was found to be 82.6% for NaOCl oxidant. The M_n, M_w, and PDI values of PNMMP and OPNMMP–EPC were found to be 1300 g/mol, 1500 g/mol, and 1.154 and 1500 g/mol, 1900 g/mol, and 1.267, respectively. The kinetics of the thermal decomposition of OPNMMP–EPC were investigated by

thermogravimetric analysis at different βs. The E values of the thermal decomposition of OPNMMP–EPC obtained by the FR, FWO, Kissinger, IKP, and CR methods under a nitrogen atmosphere were found to be 82.02, 84.20, 88.47, 79.79, and 71.06 kJ/mol, respectively. The most likely decomposition process was a D_n deceleration type in terms of the CR and master plots results. The logarithmic values of A (ln A) obtained from the master plots method and IKP method were 24.94 and 27.28. The value of ln A (s^{-1}) obtained from the IKP and master plots methods were 15.66 and 15.02. The analysis of the results obtained by the CR and master plots methods showed that the decomposition mechanism of OPNMMP–EPC under N_2 was a D_n mechanism.

References

1. Kaya, İ.; Baycan, F.; Doğan, F. J Appl Polym Sci 2009, 112, 1234.
2. Kumar, D.; Sharma, R. C. Eur Polym J 1998, 34, 1053.
3. Mamedov, B. A.; Vidadi, Y. A.; Alieva, D. N.; Ragimov, A. V. Polym Int 1997, 43, 126.
4. Anyunene, I. A.; Baltushnikas, A. N.; Liogony, B. I.; Ragimov, A. V. Abstracts of the 26th Republic Conference on Polymer Materials and Their Investigation, Vulnius, Lithuania, Moscow, Russian, 1987; p 56.
5. Ionova, E. D.; Asaturov, S. A.; Ragimov, A. V. Russ. Pat. 841,328 (1981).
6. Ragimov, G. A.; Mamedov, A. G.; Ragimov, A. V. Russ. Pat. 888,506 (1981).
7. Ehlers, G. F. L.; Fisch, K. R.; Powell, W. R. J Polym Sci Part A: Polym Chem 1969, 7, 2931.
8. Kaya, İ.; Doğan, F.; Bilici, A. Polym Int 2009, 58, 570.
9. Doğan, F.; Kaya, İ. Monomers Polym 2007, 10, 527.
10. Doğan, F.; Kaya, İ.; Bilici, A. Polym Bull 2009, 63, 267.
11. El-Shekeil, A.; Al-Khader, M.; Abu-Bakr, A. O. Synth Met 2004, 143, 147.
12. Kaya, İ.; Bilici, A.; Saçak, M. J Inorg Organomet Polym 2009, 19, 443.
13. Budrugeac, P.; Segal, E. Polym Degrad Stab 2008, 93, 1073.
14. Sahmetlioğlu, E.; Mart, H.; Yuruk, H.; Surme, Y. Chem Pap 2006, 60, 65.
15. Flynn, J.; Wall, L. Polym Lett 1966, 4, 323.
16. Ozawa, T. B. Chem Soc Jpn 1965, 38, 1881.
17. Doyle, C. J. J Appl Polym Sci 1961, 5, 285.
18. Coats, A.; Redfern, J. Nature 1964, 201, 68.
19. Nunez, L.; Fraga, F.; Villanueva, M. Polymer 2000, 41, 4635.
20. Friedman, H. L. J Polym Sci C: Polym Symp 1965, 6, 183.
21. Kissinger, H. E. Anal Chem 1957, 29, 1702.
22. Lesnikovich, A. I.; Levchik, S. V. J Therm Anal 1983, 27, 89.
23. Gotor, F. J.; Criado, J. M.; Malek, J.; Koga, N. J Therm Anal Calorim 2003, 72, 901.
24. Perez-Maqueda, L. A.; Criado, J. M.; Gotor, F. J.; Malek, J. J Phys Chem A 2002, 106, 2862.
25. Wanjun, T.; Yuwen, L.; Hen, Z.; Zhiyong, W.; Cunxin, W. J Therm Anal Cal 2003, 74, 309.
26. Atta, A. M.; Alsabagh, A. M.; Maysour, N. E.; Abdel-Azim, A. A. Prog Org Coat 2006, 56, 91.
27. Lesnikovich, A. L.; Levchik, S. V. J Propul Power 1985, 1, 311.